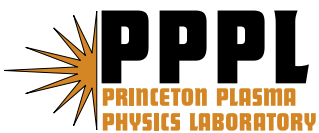


**Finite Element Implementation of Braginskii's Gyroviscous Stress  
with Application to the Gravitation Instability**

N.M. Ferraro and S.C. Jardin

May 2006



# **Princeton Plasma Physics Laboratory**

## **Report Disclaimers**

---

### **Full Legal Disclaimer**

This report was prepared as an account of work sponsored by an agency of the United States Government. Neither the United States Government nor any agency thereof, nor any of their employees, nor any of their contractors, subcontractors or their employees, makes any warranty, express or implied, or assumes any legal liability or responsibility for the accuracy, completeness, or any third party's use or the results of such use of any information, apparatus, product, or process disclosed, or represents that its use would not infringe privately owned rights. Reference herein to any specific commercial product, process, or service by trade name, trademark, manufacturer, or otherwise, does not necessarily constitute or imply its endorsement, recommendation, or favoring by the United States Government or any agency thereof or its contractors or subcontractors. The views and opinions of authors expressed herein do not necessarily state or reflect those of the United States Government or any agency thereof.

### **Trademark Disclaimer**

Reference herein to any specific commercial product, process, or service by trade name, trademark, manufacturer, or otherwise, does not necessarily constitute or imply its endorsement, recommendation, or favoring by the United States Government or any agency thereof or its contractors or subcontractors.

## **PPPL Report Availability**

---

### **Princeton Plasma Physics Laboratory**

This report is posted on the U.S. Department of Energy's Princeton Plasma Physics Laboratory Publications and Reports web site in Fiscal Year 2006.

The home page for PPPL Reports and Publications is:

[http://www.pppl.gov/pub\\_report/](http://www.pppl.gov/pub_report/)

### **Office of Scientific and Technical Information (OSTI):**

Available electronically at: <http://www.osti.gov/bridge>.

Available for a processing fee to U.S. Department of Energy and its contractors, in paper from:

U.S. Department of Energy  
Office of Scientific and Technical Information  
P.O. Box 62  
Oak Ridge, TN 37831-0062

Telephone: (865) 576-8401

Fax: (865) 576-5728

E-mail: [reports@adonis.osti.gov](mailto:reports@adonis.osti.gov)

# Finite Element Implementation of Braginskii's Gyroviscous Stress with Application to the Gravitational Instability

N. M. Ferraro and S. C. Jardin

*Princeton Plasma Physics Laboratory, Princeton, NJ 08543-0451*

## Abstract

We present a general, coordinate-independent expression for Braginskii's form of the ion gyroviscosity in the two-dimensional potential field representation, and implement this force in a full two-dimensional, two-fluid extended magnetohydrodynamic (MHD) numerical model. Our expression for the gyroviscous force requires no field to be differentiated more than twice, and thus is appropriate for finite elements with first derivatives continuous across element boundaries ( $C^1$  finite elements). We derive from our model, including the full gyroviscous stress, linear dispersion relations of a homogeneous equilibrium and of an inverted-density profile in the presence of gravity. Our treatment of the gravitational instability substantially extends previous work on the subject [1, 2]. Linear and nonlinear simulations of the gravitational instability are presented. Simulations are shown to agree closely with these dispersion relations in the linear regime. The “gyroviscous cancellation” effect is demonstrated, and some limitations of the  $\vec{v}_*$  approximation are discussed.

## I. INTRODUCTION

While MHD has been successful in describing many gross features of plasma equilibria, it is widely recognized that it is necessary to go beyond the simple ideal- or resistive-MHD models in order to calculate realistic equilibria, and to properly understand the normal modes and stability properties of these equilibria. “Extended MHD” is the name given to fluid plasma models which retain more terms than ideal- or resistive-MHD. Current numerical treatments of such models include M3D [3] and NIMROD [4]. The method we present here significantly extends the work of Jardin and Breslau [5, 6], who considered the four-field model [7], by including compressibility, density evolution, pressure evolution of both species, and Braginskii’s form of the ion gyroviscous stress in its entirety.

Although the gyroviscous stress is frequently small in magnetized plasmas, even terms which are negligible throughout most of the domain can play an important role in determining global dynamics through their effect in localized boundary layers. Magnetic reconnection in plasmas provides two important examples of this. First, the introduction of even a very small resistivity permits global topological changes which are not possible in ideal MHD (*e.g.* through the tearing mode) [8]. Second, the Hall effect, which typically plays a minor role throughout the bulk of the plasma, may completely alter the large-scale steady-state geometry of the reconnecting plasma via the introduction of dispersive waves near the “X-point” [9]. It is worth noting that the gyroviscous stress also introduces dispersive waves, and has been shown to play an important role near the X-point in kinetic simulations [10].

In general geometry, the gyroviscous stress is highly nonlinear, and involves high-order derivatives of the magnetic field and velocity variables [11]. It is therefore nontrivial to insert this term into numerical models. In section II we describe a general method for incorporating Braginskii’s form of the gyroviscous stress into a model using the two-dimensional potential field representations (defined by equations (1)), and employing  $C^1$  finite elements. The operators derived in that section are explicitly calculated for the case of polynomial basis functions in Appendix A.

In section III we describe in detail our extended-MHD model. In order to validate our code, we derive the linear dispersion relation of our model for perturbations about a homogeneous equilibrium, and show that our simulations reproduce the predicted normal modes to high accuracy. We also explore the gravitational instability, which is known to be stabilized

by gyroviscosity, in some cases even when  $k\rho_i \ll 1$  [1]. Previous work on this instability by Roberts and Taylor [2] considered the low- $\beta$ , electrostatic limit. We extend their treatment to arbitrary  $\beta$ , including the effects of electromagnetism and perturbations parallel to the gravitational force. Our simulations agree quite closely with our expanded dispersion relation in the linear regime.

Finally, we present the results of numerical simulations demonstrating the ‘‘gyroviscous cancellation’’ effect, in which one term of the gyroviscous stress has the effect of subtracting  $\vec{v}_*$  from the advective velocity in the fluid momentum equation. Often it is assumed that  $\vec{v}_*$  is the ion diamagnetic drift velocity, but  $\vec{v}_*$  should in fact be the ion magnetization velocity (defined by equation (19)) if magnetic field gradients are present [11]. The simulation results demonstrate the importance of this point. We also present a simple situation in which  $\vec{v}_* = 0$ , but  $\nabla \cdot \Pi \neq 0$ , which clearly could not be treated correctly by models which make the common approximation  $\nabla \cdot \Pi = -n\vec{v}_* \cdot \nabla \vec{v}$ .

## II. FINITE ELEMENT DECOMPOSITION

We consider a mesh of  $E$  2-dimensional finite elements, having  $D$  total basis functions, and with each element having  $N$  nonzero basis functions within its domain. The set of all independent basis functions is  $\nu_i$ , where  $i$  ranges from 1 to  $D$ . The scalar fields are represented as a linear combination of the basis functions. For example,  $U = \nu_i U_i$  (we adopt the convention that repeated indices imply summation). In this paper, we make no distinction between the projection of the field into the space spanned by the basis functions (*e.g.*  $\nu_i U_i$ ) and the field itself (*e.g.*  $U$ ). That is, we formally assume that the basis is complete.

We write the magnetic and velocity vector fields in terms of scalar potential fields

$$\vec{B} = \nabla\psi \times \hat{z} + I\hat{z} \quad (1a)$$

$$\vec{v} = \nabla U \times \hat{z} + V\hat{z} + \nabla\chi \quad (1b)$$

where  $\hat{z}$  is the unit vector in the direction of the ignorable coordinate ( $\partial_z = 0$ ).

The time evolution of the velocity field is governed by the momentum equation. For clarity, we consider only the gyroviscous contribution to this equation:

$$n \frac{\partial \vec{v}}{\partial t} = -\nabla \cdot \Pi + \dots \quad (2)$$

We now apply the operators  $-\hat{z} \cdot \nabla \times$ ,  $\hat{z} \cdot$ , and  $\nabla \cdot$  to this equation to obtain the equations governing the time evolution of the scalar velocity fields. For example, in the case of constant density, we would have:

$$n \nabla^2 \dot{U} = \hat{z} \cdot \nabla \times (\nabla \cdot \Pi) \quad (3a)$$

$$n \dot{V} = -\hat{z} \cdot (\nabla \cdot \Pi) \quad (3b)$$

$$n \nabla^2 \dot{\chi} = -\nabla \cdot (\nabla \cdot \Pi). \quad (3c)$$

Applying the Galerkin method, we multiply both sides by each basis function  $\nu_i$ , and integrate over the domain. Integrating equations (3) by parts, and allowing the boundary terms to vanish, yields

$$-\int dA \nabla(\nu_i n) \cdot \nabla \dot{U} = \int dA \varepsilon_{z\rho\nu} (\partial_\mu \partial_\rho \nu_i) \Pi_{\mu\nu} \quad (4a)$$

$$\int dA \nu_i n \dot{V} = \int dA \nabla \nu_i \cdot (\Pi \cdot \hat{z}) \quad (4b)$$

$$-\int dA \nabla(\nu_i n) \cdot \nabla \dot{\chi} = -\int dA (\nabla \nabla \nu_i) : \Pi, \quad (4c)$$

where  $\varepsilon$  is the Levi-Civita tensor, and Greek subscripts index spatial vector components. The integrations by parts are done to move derivatives off of  $\Pi$ , which by itself involves the second derivative of the velocity fields  $U$  and  $\chi$ . This reduces the order of the differential operators to two, which can be handled by  $C^1$  finite-elements without further approximation [5].

In the following discussion we use the convenient tensor notation where  $a_{\mu,\nu} = \partial_\nu a_\mu$ , and where square brackets (parentheses) represent anti-symmetrization (symmetrization) over the enclosed subscripts. For example,  $a_{,[x}b_{,y]}$   $= a_{,x}b_{,y} - a_{,y}b_{,x}$ . This particular combination is frequently written  $[a, b]$  in the MHD literature. Note that anti-symmetrization over  $x$  and  $y$  produces quantities which are invariant to rotations about  $\hat{z}$ —that is, they are coordinate-invariant in two dimensions. Similarly, contraction of indices (as in  $a_\mu b_\mu$ ) produces coordinate-invariant scalars. The complicated symmetries of terms in the following expressions make it necessary to adopt this notation in order to write all of the terms in the following tensors in a compact, manifestly coordinate-independent way.

We now insert the explicit form of Braginskii's gyroviscous stress tensor for  $\Pi$  [11, 12]

$$\Pi_{\mu\nu} = \frac{p^{(i)}}{4B^2} \varepsilon_{\rho\sigma(\mu} \left[ \delta_{\nu)\tau} + 3 \frac{B_\nu B_\tau}{B^2} \right] B_\rho v_{(\sigma,\tau)} \quad (5)$$

where  $p^{(i)}$  is the perpendicular ion pressure (in this paper we do not consider anisotropic pressure). Note that in this notation,  $\Pi$  is manifestly symmetric. The integrands of the right-hand sides of equations (4) can be written:

$$\frac{p^{(i)}}{2B^2} \left\{ \begin{aligned} & I \left( 2 + 3 \frac{\psi_{,\mu}\psi_{,\mu}}{B^2} \right) \nu_{i,\nu} [xU]_{,\nu} + \\ & + \frac{1}{2} \left[ \left( 1 - 3 \frac{I^2}{B^2} \right) (\psi_{,[x\nu_{i,y]\mu} V_{,\mu}} + V_{,[x\nu_{i,y]\mu} \psi_{,\mu}}) - \frac{3}{B^2} \psi_{,[xV_{,y]} (\nu_{i,\mu\mu} \psi_{,\nu} \psi_{,\nu} + 2\psi_{,[x\nu_{i,y][x\psi_{,y]}}) \right] + \end{aligned} \right\} \quad (6a)$$

$$\frac{p^{(i)}}{2B^2} \left\{ \begin{aligned} & \frac{1}{2} \left[ \left( 1 - 3 \frac{I^2}{B^2} \right) (\psi_{,[xU_{,y]\mu} \nu_{i,\mu}} + \nu_{i,[xU_{,y]\mu} \psi_{,\mu}}) - \frac{3}{B^2} \psi_{,[x\nu_{i,y]} (U_{,\mu\mu} \psi_{,\nu} \psi_{,\nu} + 2\psi_{,[xU_{,y][x\psi_{,y]}}) \right] - \\ & - \frac{1}{2} I \left( 1 + 3 \frac{I^2 - \psi_{,\mu}\psi_{,\mu}}{B^2} \right) \nu_{i,[xV_{,y]} + \end{aligned} \right\} \quad (6b)$$

$$\frac{p^{(i)}}{2B^2} \left\{ \begin{aligned} & + \nu_{i,\mu} \chi_{,\mu\nu} \psi_{,\nu} + \frac{3}{B^2} (\psi_{,[x\nu_{i,y]} \psi_{,[x\chi_{,y]\mu} \psi_{,\mu}} - I^2 \nu_{i,[x\chi_{,y][x\psi_{,y]}}) \\ & - I \left[ \left( 2 + 3 \frac{\psi_{,\mu}\psi_{,\mu}}{B^2} \right) U_{,\nu\rho} \nu_{i,\nu\rho} - \left( 1 + 3 \frac{\psi_{,\mu}\psi_{,\mu}}{B^2} \right) U_{,\nu\nu} \nu_{i,\rho\rho} - \frac{3}{B^2} \psi_{,[xU_{,y][x\psi_{,y]} \nu_{i,\mu\mu}} \right] + \\ & + V_{,\mu} \nu_{i,\mu\nu} \psi_{,\nu} + \frac{3}{B^2} (\psi_{,[xV_{,y]} \psi_{,[x\nu_{i,y]\mu} \psi_{,\mu}} - I^2 V_{,[x\nu_{i,y][x\psi_{,y]}}) + \\ & + I \left[ \left( 2 + 3 \frac{\psi_{,\mu}\psi_{,\mu}}{B^2} \right) \nu_{i,\nu} [x\chi_{,y]\nu} - \frac{3}{B^2} (\nu_{i,\mu\mu} \psi_{,[x\chi_{,y]\nu} \psi_{,\nu}} - \chi_{,\mu\mu} \psi_{,[x\nu_{i,y]\nu} \psi_{,\nu}}) \right] \end{aligned} \right\} \quad (6c)$$

We now seek to write equations (4) in the form:

$$0 = \begin{pmatrix} L_{ij}^{11} & L_{ij}^{12} & L_{ij}^{13} \\ L_{ij}^{21} & L_{ij}^{22} & L_{ij}^{23} \\ L_{ij}^{31} & L_{ij}^{32} & L_{ij}^{33} \end{pmatrix} \begin{pmatrix} \dot{U}_j \\ \dot{V}_j \\ \dot{\chi}_j \end{pmatrix} + \begin{pmatrix} R_{ij}^{11} & R_{ij}^{12} & R_{ij}^{13} \\ R_{ij}^{21} & R_{ij}^{22} & R_{ij}^{23} \\ R_{ij}^{31} & R_{ij}^{32} & R_{ij}^{33} \end{pmatrix} \begin{pmatrix} U_j \\ V_j \\ \chi_j \end{pmatrix} \quad (7)$$

Here we have written  $(U_j \ V_j \ \chi_j)^T$  as shorthand for the vector  $(U_1 \ \dots \ U_D \ V_1 \ \dots \ V_D \ \chi_1 \ \dots \ \chi_D)^T$ , and so each  $L_{ij}^{ab}$  and  $R_{ij}^{ab}$  is an  $D \times D$  block. We write this system equations succinctly as

$$0 = \vec{L}_i \cdot \vec{\dot{V}} + \vec{R}_i \cdot \vec{V}, \quad (8)$$

At this point,  $\vec{L}$  and  $\vec{R}$  must be viewed as linear integro-differential operators on  $\vec{V}$ . For example, in the case where density is constant,  $L_{ij}^{11} U_j = - \int dA \nabla(\nu_i n) \cdot \nabla U$ . However, the differentiations and integrations can be carried out explicitly once the actual forms of the basis functions are inserted, and equation (8) becomes an algebraic matrix equation. An example is worked out in the appendix.

### A. 4<sup>th</sup> rank Decomposition of $\vec{R}$

A difficulty is that the elements of  $\vec{R}$  each involve products of between three and five field variables, including the basis function. When contracted with the velocity field vector  $\vec{V}$ , this increases the order of the nonlinearity to six. Since each field variable is itself represented as a linear combination of basis functions having  $N$  terms, computing a sixth-order nonlinear term involves computing a sum of  $N^6$  terms (neglecting possible symmetry considerations). In this context, the computation is actually the contraction of a sixth-rank tensor, potentially having  $N^6$  elements, with basis function expansion of six field variables. These facts raise computational memory and speed issues, which are multiplied again by the number of finite elements.

In order to circumvent this problem, we rewrite the elements of  $\vec{R}$  in terms of fourth-rank tensors only, which results in a significant (factor of  $N^2$ ) memory and speed advantage. In order to do this, we define common products of fields as new ‘‘auxiliary fields.’’ These auxiliary fields, defined below, must not contain the velocity field variable or the trial function, since these fields are not contracted in equation (8).

A slight complication introduced by this process is that we necessarily break up the elements of  $\vec{R}$  into pieces which are not all individually coordinate-invariant. (Note that the elements of  $\vec{L}$  and  $\vec{R}$  must be coordinate-invariant.) This causes the final expressions for the coordinate-specific tensors to contain explicitly the orientation of the finite element. However, it does not impose any limitation on the orientations of the finite elements, or contribute any significant difficulty to the calculation of the matrices.

We define the following auxiliary fields:

$$\begin{aligned} Y^{(1)} &= p^{(i)}/B^2 \\ Y^{(2)} &= 3Y^{(1)}/B^2 \\ Y^{(3)} &= Y^{(2)}I^2 \\ Y^{(4)} &= Y^{(2)}\psi_{,\nu}\psi_{,\nu}/2 \\ Y^{(5)} &= Y^{(2)}(\psi_{,x}^2 - \psi_{,y}^2)/2 \\ Y^{(6)} &= Y^{(2)}\psi_{,x}\psi_{,y}. \end{aligned}$$

These variables must also be projected into the space spanned by the basis functions, so  $Y^{(1)} = \nu_i Y_i^{(1)}$ , for example. Note that  $Y^{(1)}$ ,  $Y^{(2)}$ ,  $Y^{(3)}$ , and  $Y^{(4)}$  are coordinate-invariant,

whereas  $Y^{(5)}$  and  $Y^{(6)}$  are not.

The individual elements of  $\overleftrightarrow{R}$  can be written:

$$\begin{aligned}
R_{ij}^{11} &= G_{ijkl}^{(11a)} I_k (Y_l^{(1)} + Y_l^{(4)}) \\
R_{ij}^{12} &= G_{ijkl}^{(12a)} \psi_k (Y_l^{(1)} - Y_l^{(3)}) + G_{ijkl}^{(12b)} \psi_k Y_l^{(5)} + G_{ijkl}^{(12c)} \psi_k Y_l^{(6)} \\
R_{ij}^{13} &= G_{ijkl}^{(13a)} I_k (Y_l^{(1)} + Y_l^{(4)}) + G_{ijkl}^{(13b)} I_k Y_l^{(5)} + G_{ijkl}^{(13c)} I_k Y_l^{(6)} \\
R_{ij}^{21} &= G_{jikl}^{(12a)} \psi_k (Y_l^{(1)} - Y_l^{(3)}) + G_{jikl}^{(12b)} \psi_k Y_l^{(5)} + G_{jikl}^{(12c)} \psi_k Y_l^{(6)} \\
R_{ij}^{22} &= G_{ijkl}^{(22a)} I_k (Y_l^{(1)} + Y_l^{(3)} - 2Y_l^{(4)}) \\
R_{ij}^{23} &= G_{ijkl}^{(23a)} \psi_k Y_l^{(1)} + G_{ijkl}^{(23b)} \psi_k Y_l^{(3)} - G_{jikl}^{(12c)} \psi_k Y_l^{(5)} + G_{jikl}^{(12b)} \psi_k Y_l^{(6)} \\
R_{ij}^{31} &= -G_{ijkl}^{(13a)} I_k (Y_l^{(1)} + Y_l^{(4)}) - G_{jikl}^{(13b)} I_k Y_l^{(5)} - G_{jikl}^{(13c)} I_k Y_l^{(6)} \\
R_{ij}^{32} &= G_{jikl}^{(23a)} \psi_k Y_l^{(1)} + G_{jikl}^{(23b)} \psi_k Y_l^{(3)} - G_{ijkl}^{(12c)} \psi_k Y_l^{(5)} + G_{ijkl}^{(12b)} \psi_k Y_l^{(6)} \\
R_{ij}^{33} &= G_{ijkl}^{(11a)} I_k (Y_l^{(1)} + Y_l^{(4)}) + G_{ijkl}^{(33b)} I_k Y_k^{(5)} + G_{ijkl}^{(33c)} I_k Y_k^{(6)}
\end{aligned}$$

where  $G$  operators have been defined as follows:

$$\begin{aligned}
G_{ijkl}^{(11a)} B_j C_k D_l &= -\nu_{i,\mu[xB,y]\mu} C D \\
G_{ijkl}^{(12a)} B_j C_k D_l &= -\frac{1}{2} (C_{,[x\nu_{i,y]\mu} B_{,\mu} + B_{,[x\nu_{i,y]\mu} C_{,\mu}) D \\
G_{ijkl}^{(12b)} B_j C_k D_l &= \frac{1}{2} C_{,[xB,y]} (\nu_{i,xx} - \nu_{i,yy}) D \\
G_{ijkl}^{(12c)} B_j C_k D_l &= C_{,[xB,y]} (\nu_{i,xy}) D \\
G_{ijkl}^{(13a)} B_j C_k D_l &= -\left( \nu_{i,\mu\nu} B_{,\mu\nu} + \frac{1}{2} \nu_{i,\mu\mu} B_{,\nu\nu} \right) C D \\
G_{ijkl}^{(13b)} B_j C_k D_l &= \frac{1}{2} B_{,\mu\mu} (\nu_{i,xx} - \nu_{i,yy}) C D \\
G_{ijkl}^{(13c)} B_j C_k D_l &= B_{,\mu\mu} (\nu_{i,xy}) C D \\
G_{ijkl}^{(22a)} B_j C_k D_l &= \frac{1}{4} \nu_{i,[xB,y]} C D \\
G_{ijkl}^{(23a)} B_j C_k D_l &= -\frac{1}{2} \nu_{i,\mu} B_{,\mu\nu} C_{,\nu} D \\
G_{ijkl}^{(23b)} B_j C_k D_l &= \frac{1}{2} \nu_{i,[xB,y][xC,y]} D \\
G_{ijkl}^{(33b)} B_j C_k D_l &= (\nu_{i,\mu\mu} B_{,xy} - B_{,\mu\mu} \nu_{i,xy}) C D \\
G_{ijkl}^{(33c)} B_j C_k D_l &= (\nu_{i,xx} B_{,yy} - \nu_{i,yy} B_{,xx}) C D
\end{aligned}$$

Note that contraction over the fourth index is always equivalent to scalar multiplication, as contraction over the third index often is. Also note that all the operators containing “ $a$ ” in the superscript are coordinate invariant, but the ones containing “ $b$ ” and “ $c$ ” are not. Comparing these definitions with the definitions of  $\vec{R}$ , it is readily seen that  $B$  will always be one of the velocity variables  $U$ ,  $V$ , or  $\chi$ ;  $C$  will always be one of the magnetic field variables  $\psi$  or  $I$ ; and  $D$  will always be a linear combination of the auxiliary variables.

### III. MODEL DESCRIPTION, APPLICATIONS, AND SIMULATION RESULTS

We have developed a numerical code which solves the full “eight-field” extended-MHD model in 2D cylindrical slab geometry. The eight-field model is so named because  $U$ ,  $V$ ,  $\chi$ ,  $\psi$ ,  $I$ ,  $n$ ,  $p^{(e)}$  and  $p$  are evolved in time. In units normalized to an arbitrary density  $\bar{n}$  and magnetic field strength  $\bar{B}$ , where time and distance are normalized respectively to the inverse ion gyrofrequency  $\bar{\Omega}_i^{-1} = m_i c / e \bar{B}$  and ion skin depth  $\bar{d}_i = c \sqrt{m_i / 4\pi \bar{n} e^2}$ , this model is:

$$\begin{aligned}
\frac{\partial n}{\partial t} &= -\nabla \cdot (n\vec{v}) \\
\frac{\partial \vec{B}}{\partial t} &= -\nabla \times \vec{E} \\
n \frac{\partial \vec{v}}{\partial t} &= -n\vec{v} \cdot \nabla \vec{v} + \vec{J} \times \vec{B} - \nabla p - \nabla \cdot \Pi^{(i)} + \\
&\quad + n\vec{g} + \mu \nabla^2 \vec{v} \\
\frac{\partial p^{(e)}}{\partial t} &= -\nabla \cdot (p^{(e)}\vec{v}) - \\
&\quad - (\Gamma - 1) [p^{(e)}\nabla \cdot \vec{v} + \nabla \cdot \vec{q}^{(e)} - Q_\Delta] + \\
&\quad + \frac{\vec{J}}{n} \cdot \left( \nabla p^{(e)} - \Gamma p^{(e)} \frac{\nabla n}{n} + (\Gamma - 1)\vec{R} \right) \\
\frac{\partial p}{\partial t} &= -\nabla \cdot (p\vec{v}) - \\
&\quad - (\Gamma - 1) [p\nabla \cdot \vec{v} + \nabla \cdot (\vec{q}^{(i)} + \vec{q}^{(e)})] + \\
&\quad + \frac{\vec{J}}{n} \cdot \left( \nabla p^{(e)} - \Gamma p^{(e)} \frac{\nabla n}{n} + (\Gamma - 1)\vec{R} \right)
\end{aligned}$$

where

$$\begin{aligned}
\vec{E} + \vec{v} \times \vec{B} &= \frac{1}{n} \left( \vec{R} + \vec{J} \times \vec{B} - \nabla p^{(e)} \right) \\
\vec{J} &= \nabla \times \vec{B}; \quad p = p^{(i)} + p^{(e)},
\end{aligned}$$

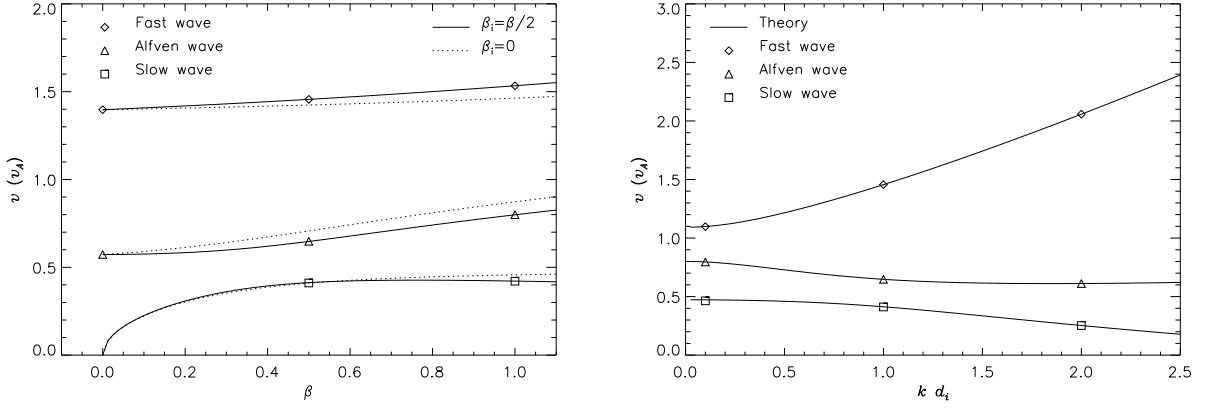


FIG. 1: The measured phase velocity is plotted over the linear theory results (solid lines). The data points are computed with  $p^{(i)} = p/2$ . *Left:*  $k = 1$ , and  $\beta$  is varied. Also plotted is the theoretical phase velocity with  $p^{(i)} = 0$  (dotted line). *Right:*  $\beta = 0.5$ , and  $k$  is varied. In both figures, error in measuring the phase velocity is smaller than the plotting symbol size.

and  $\Gamma$  is the ratio of specific heats. The rate of momentum transfer between species is taken to be proportional to the plasma current:  $\vec{R} = \eta n \vec{J}$ ; the rate of heat transfer between species is  $Q_{\Delta} = 3(m_e/m_i)(p - 2p^{(e)})/\tau_e$ , where  $\tau_e$  is the electron-ion collision time.

Our numerical method is the same as that used by Jardin and Breslau [6]. We use high-order  $C^1$  finite-elements [5] with the split semi-implicit method [6] applied to the MHD terms and a  $\theta$ -implicit evaluation of the gyroviscous term, where  $\theta = 1$  corresponds to a fully implicit time step, and  $\theta = 1/2$  corresponds to centered time derivatives.

## A. Normal Modes in an Infinite, Homogeneous Equilibrium

The normal modes are found for plane wave perturbations about a stationary, homogeneous equilibrium:

$$\begin{aligned}
\psi(\vec{r}, t) &= B_{x0}y + \epsilon\psi_1 e^{i(\vec{k}\cdot\vec{r}-\omega t)} \\
I(\vec{r}, t) &= I_0 + \epsilon I_1 e^{i(\vec{k}\cdot\vec{r}-\omega t)} \\
U(\vec{r}, t) &= \epsilon U_1 e^{i(\vec{k}\cdot\vec{r}-\omega t)} \\
V(\vec{r}, t) &= \epsilon V_1 e^{i(\vec{k}\cdot\vec{r}-\omega t)} \\
\chi(\vec{r}, t) &= \epsilon \chi_1 e^{i(\vec{k}\cdot\vec{r}-\omega t)} \\
p(\vec{r}, t) &= p_0 + \epsilon p_1 e^{i(\vec{k}\cdot\vec{r}-\omega t)} \\
p^{(e)}(\vec{r}, t) &= p_0^{(e)} + \epsilon p_1^{(e)} e^{i(\vec{k}\cdot\vec{r}-\omega t)} \\
n(\vec{r}, t) &= n_0 + \epsilon n_1 e^{i(\vec{k}\cdot\vec{r}-\omega t)}.
\end{aligned}$$

The normal modes are found to first order in the ordering parameter  $\epsilon$ . We do not consider the damping effects introduced by dissipative terms ( $\mu = \eta = 0$ ). In the case that  $\vec{k} = k_x \hat{x}$ , we find the linear dispersion relation of this system to be exactly

$$0 = (a_3 \bar{\omega}^6 + a_2 \bar{\omega}^4 + a_1 \bar{\omega}^2 + a_0) \bar{\omega}^2 \quad (9)$$

where

$$\begin{aligned}
a_3 &= -1 \\
a_2 &= 1 + b_k^2 + \bar{\beta} + \bar{\nu}^2(1 + 6b_k^2 - 3b_k^4) + \frac{b_k^2}{\bar{\Omega}^2} \\
a_1 &= -b_k^2 \left\{ 1 + 2\bar{\beta} - 2\frac{\bar{\nu}}{\bar{\Omega}}(1 + b_k^2) + \bar{\nu}^2 [4(1 - b_k^2) + \bar{\beta}(1 - 3b_k^2)^2] + \frac{1}{\bar{\Omega}^2} [\bar{\beta} + \bar{\nu}^2(1 + 6b_k^2 - 3b_k^4)] \right\} \\
a_0 &= b_k^4 \bar{\beta} \left[ 1 + \frac{\bar{\nu}}{\bar{\Omega}}(1 - 3b_k^2) \right]^2.
\end{aligned}$$

Here we have defined the following quantities:  $B^2 = B_{x0}^2 + I_0^2$ ;  $b_k = B_{x0}/B$ ;  $\bar{\beta} = \Gamma p_0/B^2 = \Gamma\beta/2$  is the ratio of the sound speed to the Alfvén speed;  $v_A = B/\sqrt{n_o}$  is the Alfvén speed;  $\bar{\omega} = \omega/kv_A$ ;  $\bar{\Omega} = \Omega_i/kv_A$  is the normalized ion gyrofrequency, and is present only in terms due to the Hall effect; and  $\bar{\nu} = \rho_i^2 \Omega_i k / 2v_A$  is present only in terms due to gyroviscosity. In our system of units,  $\Omega_i = B$  and  $\rho_i^2 = p_0^{(i)}/n_0 B^2$ . For the eigenmodes with  $\bar{\omega} \neq 0$ , the

perturbed fields are related in the following way:

$$\bar{U}_1 = -\frac{b_k}{\bar{\omega}} \frac{\bar{\omega}^2(\bar{\omega}^2 - \bar{\beta}) - \bar{\omega}^2 + b_k^2\bar{\beta} + \bar{\nu} [\bar{\omega}^2(1 + b_k^2) + b_k^2(1 - 3b_k^2)\bar{\beta}]}{(\bar{\omega}^2 - 1)(\bar{\omega}^2 - \bar{\beta}) - (1 - b_k^2)\bar{\beta} - \bar{\nu}^2 [\bar{\omega}^2(1 + 6b_k^2 - 3b_k^4) - 4b_k^2(1 - b_k^2) - b_k^2(1 - 3b_k^2)^2\bar{\beta}]} / \bar{\Omega} \quad (10a)$$

$$\bar{V}_1 = -b_k \frac{b_k(\bar{\omega}^2 - \bar{\beta})\bar{\psi}_1/\bar{\Omega} - \bar{\nu}\bar{\omega} [2(1 - b_k^2) - (\bar{\omega}^2 - \bar{\beta})(1 - 3b_k^2)] \bar{U}_1}{(\bar{\omega}^2 - 1)(\bar{\omega}^2 - \bar{\beta}) - (1 - b_k^2)\bar{\beta}} \quad (10b)$$

$$\bar{I}_1 = -\frac{b_k(\bar{\omega}^2 - \bar{\beta})(\bar{V}_1 - \bar{\psi}_1/\bar{\Omega})/\bar{\omega} + \bar{\nu}(1 - b_k^2)(1 + 3b_k^2)\bar{U}_1}{(\bar{\omega}^2 - \bar{\beta}) - (1 - b_k^2)} \quad (10c)$$

$$\bar{\chi}_1 = -\frac{I_0/B}{\bar{\omega}^2 - \bar{\beta}} [\bar{\nu}(1 + 3b_k^2)\bar{U}_1 - \bar{I}_1] \quad (10d)$$

$$n_1 = n_0\bar{\chi}_1 \quad (10e)$$

$$p_1 = \Gamma p_0\bar{\chi}_1 \quad (10f)$$

$$p_1^{(e)} = \Gamma p_0^{(e)}\bar{\chi}_1. \quad (10g)$$

Here we have defined the non-dimensional quantities  $\bar{U}_1 = kU_1/v_A$ ,  $\bar{V}_1 = V_1/v_A$ ,  $\bar{I}_1 = I_1/B$ , and  $\bar{\chi}_1 = ik\chi_1/\bar{\omega}v_A$ .

Formally there are eight solutions to the dispersion relation, equation (9). Since  $\omega$  enters only in even powers, for each of the positive eigenvalues there will be a corresponding negative eigenvalue of equal magnitude. Two of the eigenvalues are zero; these correspond to stationary density and pressure perturbations. The remaining six eigenvalues correspond to the shear Alfvén, slow magnetosonic and fast magnetosonic waves (which may each propagate parallel or anti-parallel to the magnetic field). The equilibrium is linearly stable, so all eigenvalues are real. When  $\bar{\nu} \neq 0$ , there are no longer purely compressible or incompressible wave solutions; this fact is due to issues raised in section III C.

We simulate these waves by finding the eigenvalues  $\omega$  from equation (9), and initializing a perturbation using the corresponding eigenvector determined by equations (10). The parameters for these simulations are:  $p_0 = 0.25$ ,  $p_0^{(i)} = 0.125$ ,  $B_{x0} = 0.8$ ,  $I_0 = 0.6$ ,  $\Gamma = 5/3$ ,  $\mu = 0.001$ ,  $\eta = 0.001$ ,  $\epsilon = 10^{-4}$ , and  $\theta = 0.5$ . The simulation domain is doubly periodic with  $L_x = 2\pi/k$  and  $L_y = 1$ , on a mesh with 100 elements. Phase velocities are determined by measuring the velocity of the wave crest over the duration of the simulation. Wave velocities of each wave are plotted versus  $\beta = 2p_0/B^2$  and  $k$  in figure 1.

The difference between the measured phase velocities and the theoretical phase velocity is plotted versus the time step  $\Delta t$  in figure 2, along with the best-fit curves of the form  $f_1(\Delta t)^{f_2} + f_3$ . The values of  $f_2$  indicate that the fast wave converges approximately as  $(\Delta t)^2$ , while the slow and Alfvén waves converge approximately as  $\Delta t$ . The values of  $f_3$

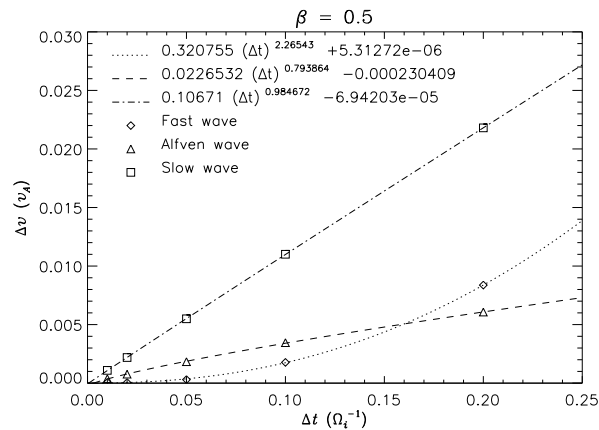


FIG. 2: Shown is the difference between the measured phase velocity and the theoretical phase velocity, as a function of the time step. The broken lines represent the best-fit curves to the data.

show that the fast wave converges more accurately than the other waves. Both of these facts are due to the the fast wave being fastest wave in the system, and small errors in the eigenvectors of the other waves will excite the fast wave.

## B. Gravitational Instability

In this section we consider an isothermal plasma in a uniform gravitational field,  $\vec{g} = -g\hat{y}$ , having a density gradient opposite to the gravitational field. Equilibria having such an inverted density profile are unstable in the ideal limit. Schnack has suggested [13] that this gravitational instability be used to validate the implementation of the gyroviscous force in extended-MHD codes, because of the severe and well-characterized effect of ion gyroviscosity on its growth rate in the linear regime. Rosenbluth, Krall and Rostoker [1] were the first to calculate, by kinetic analysis, the stabilizing effect on this instability of finite Larmor radius effects at high wavenumbers. Roberts and Taylor [2] recovered Rosenbluth *et al.*'s result in the fluid formalism by including the gyroviscous term. Both groups assume  $k_y = 0$ , and consider only the low- $\beta$  limit in order to justify the electrostatic assumption. Starting from an equilibrium with  $n(y) = e^{y/L^n}$  and a uniform  $I$ , Roberts and Taylor's result is the local linear dispersion relation:

$$0 = \bar{\omega}^2 + (2\bar{\nu} + 1/\bar{\Omega})\bar{\omega} + 1, \quad (11)$$

where

$$\bar{\omega} = \frac{\bar{\omega}}{\sqrt{\bar{g}}} \frac{k^2 L_n}{k_x} = \frac{k\omega}{k_x \sqrt{g/L_n}} \quad (12a)$$

$$\bar{\Omega} = \frac{\bar{\Omega}}{\sqrt{\bar{g}}} = \frac{\Omega_i}{k\sqrt{gL_n}} \quad (12b)$$

$$\bar{\nu} = \frac{\bar{\nu}}{\sqrt{\bar{g}}} = \frac{\rho_i^2 \Omega_i k}{2\sqrt{gL_n}}. \quad (12c)$$

(Roberts and Taylor's original definition of  $\bar{\nu}$  is half of ours, because they assume  $p^{(i)} = p/2$ . For proper comparison with our results, which are obtained under the assumption that  $p^{(i)} = p$ , we use our definition of  $\bar{\nu}$  in their dispersion relation. Also, strictly speaking, Roberts and Taylor's result is equation (11) evaluated at  $k = k_x$ .) Here  $\bar{g} = gL_n/v_A^2$  is the normalized gravitational force. Again, the term due to gyroviscosity is proportional to  $\bar{\nu}$  and the term due to the Hall effect is proportional to  $\bar{\Omega}^{-1}$ .

Equation (11) elegantly shows that both gyroviscosity and the Hall term may independently stabilize the gravitational instability. Physically, the gyroviscous stabilization is due to the fact that gyroviscosity transports the  $y$ -directed momentum across the  $x$ -direction—that is, it transfers some vertical momentum from upward-flowing regions into downward-flowing regions, and vice-versa [1, 14]. The stabilization due to the Hall term results from the electrons sweeping the magnetic field perturbations out of phase with the fluid velocity perturbations.

### 1. Linear Theory

Schnack pointed out [13] that it is necessary for the equilibrium to be supported by a magnetic field gradient, and not a thermal pressure gradient, in order to ensure that  $\partial p/\partial n$  is positive definite. Therefore we use the following equilibrium:

$$n(y) = n_0 e^{y/L_n} \quad (13a)$$

$$p(y) = Tn(y) \quad (13b)$$

$$I(y) = \sqrt{I_0^2 - 2(gL_n + \Gamma T)[n(y) - n_0]}. \quad (13c)$$

For simplicity we assume that  $p = p^{(i)}$ . We choose to work in the limit where  $kL_n \sim \delta^{-1}$  and  $\bar{g} \sim 1$ , where  $\delta \ll 1$ . The former limit corresponds to the case where the equilibrium gradient scale length is large compared to the perturbation scale length, and is necessary in

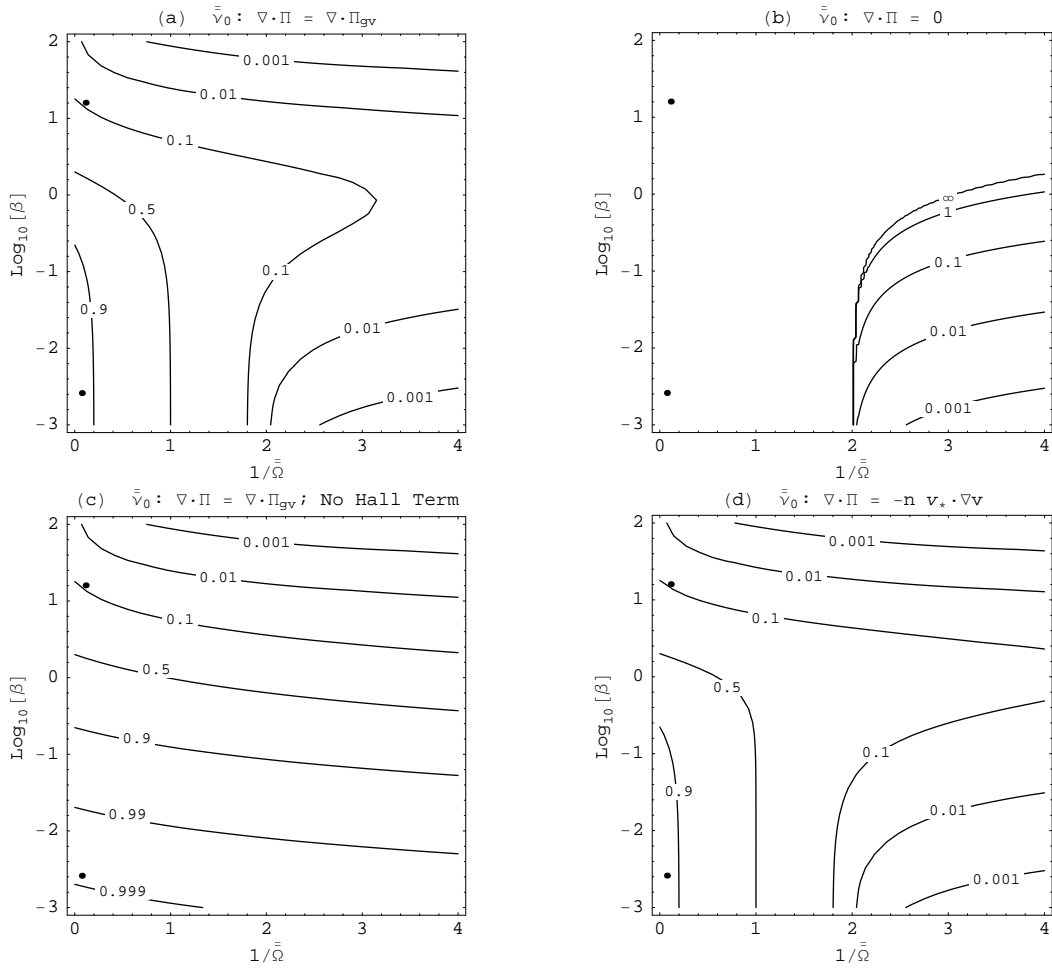


FIG. 3: Contours of the value of  $\bar{\nu}$  for which the gravitational mode is stabilized are shown, for four different models. The two points on the left of each graph represent the cutoffs of cases simulated in section III B 2. (a) Complete model using the full Braginskii form of  $\nabla \cdot \Pi$ , and including the Hall term. (b)  $\nabla \cdot \Pi = 0$ . (c) Full form of  $\nabla \cdot \Pi$ , the but the Hall term is excluded. (d)  $\nabla \cdot \Pi = -n \vec{v}_* \cdot \nabla \vec{v}$ , where  $\vec{v}_*$  is the magnetization velocity, given by equation (19).

order to justify any local analysis of the eigenmodes. The latter limit represents our choice to focus on equilibria in which the ideal growth rate of the gravitational instability is on the order of the Alfvén transit time across a gradient scale length. We consider perturbations with space and time dependence of the form  $\exp[i(k_x x + k_y y - \omega t)]$ , which is the form of the eigenmode to lowest order in  $\delta$ . We allow  $k_y \neq 0$  in order to accommodate the Dirichlet boundary conditions at  $y = \pm L_y/2$  of our simulation domain. The gravitational mode can be isolated by further choosing the frequency to be on the order of the ideal growth rate,

$\omega \sim \sqrt{g/L_n} \sim \delta$ . Given this ordering, to lowest order in  $\delta$  we find the dispersion relation to be:

$$\begin{aligned}
0 = & 1 + \left(1 + 2\frac{\bar{\bar{\nu}}}{\bar{\bar{\Omega}}}\right) (\bar{g} + \bar{\beta}) - \\
& - \left[2\bar{\nu} (1 + \bar{g} + \bar{\beta}) (1 + \bar{\beta}) + 2\bar{\nu}\bar{g} + \frac{1 - \bar{\nu}^2}{\bar{\bar{\Omega}}}\right] \bar{\omega} + \\
& + (1 + \bar{\beta} + \bar{\nu}^2\bar{g}) \bar{\omega}^2.
\end{aligned} \tag{14}$$

This equation is useful for comparison with the simulations presented in section III B 2 where, in one case,  $k\rho_i$  approaches unity. However, the Braginskii form of the gyroviscous stress is derived under the assumption of small Larmor radii [11], and it is possible that equation (14) predicts unphysical behavior when the limit  $k\rho_i \ll 1$  is violated. Applying this limit yields

$$\begin{aligned}
0 = & 1 + \bar{g} + \bar{\beta} - \\
& - \left[2\bar{\nu} (1 + \bar{g} + \bar{\beta}) (1 + \bar{\beta}) + 2\bar{\nu}\bar{g} + \frac{1}{\bar{\bar{\Omega}}}\right] \bar{\omega} + \\
& + (1 + \bar{\beta}) \bar{\omega}^2.
\end{aligned} \tag{15}$$

Equation (11) is recovered from this dispersion relation in the limit where  $\beta \ll 1$  and  $\bar{g} \ll 1$ .

The introduction of the double-overbarred quantities elucidates the fact that equation (15) contains only three independent dimensionless parameters:  $\bar{\nu}$ ,  $\bar{\bar{\Omega}}$ , and  $\bar{\beta}$ . Note that  $\bar{g}$  is not an independent parameter, since  $\bar{g} = \bar{\beta}/(2\Gamma\bar{\nu}\bar{\bar{\Omega}})$ . However, in equation (15) we do not write  $\bar{g}$  in terms of  $\bar{\bar{\Omega}}$  and  $\bar{\nu}$  so as not to imply that terms containing  $\bar{g}$  are due to the Hall effect or the gyroviscous force.

Now, using the fact that  $\bar{g}$  is a dependent quantity, we are able to calculate the value of  $\bar{\nu}$  at which the gravitational mode is stabilized as a function of the other two independent parameters,  $\beta = 2\bar{\beta}/\Gamma$  and  $\bar{\bar{\Omega}}$ . Contours of these values are shown in figure 3, using four different models.

Figure 3a shows the cutoff value of  $\bar{\nu}$  for the full dispersion relation, equation (15). Figure 3b shows the cutoff value of  $\bar{\nu}$  in the absence of gyroviscosity. From that figure, it can be seen that the Hall term is responsible for stabilizing modes having both  $\beta \ll 1$  and  $1/\bar{\bar{\Omega}} \gtrsim 2$ , but does not stabilize modes outside this region of parameter space. Figure 3c shows the case where gyroviscosity is retained, but the Hall term is instead omitted; there it can be seen that the gyroviscous stress independently stabilizes all modes at  $\bar{\nu} = 1$ , and is especially stabilizing to modes with high  $\beta$ . Note that the mode can be stabilized by

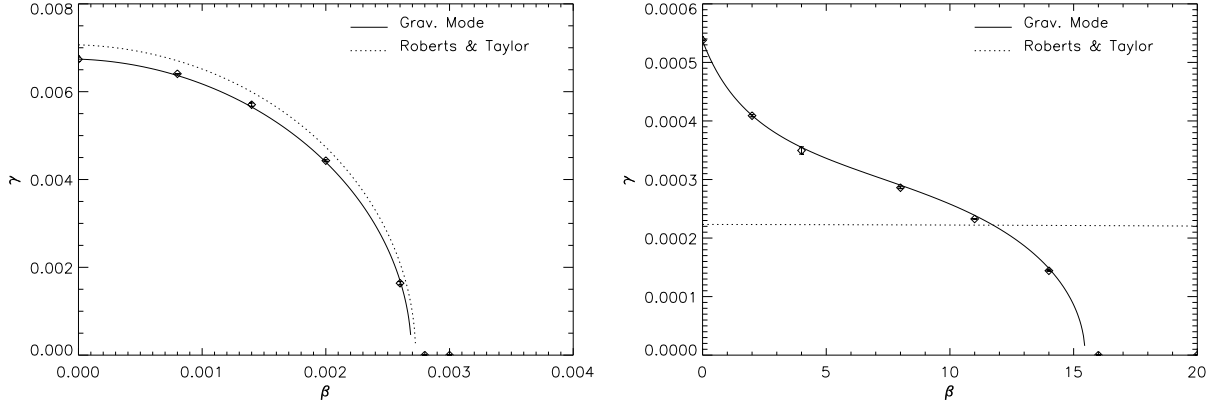


FIG. 4: Simulation results are plotted against the solutions to equation (14) and Roberts and Taylor’s result, equation (11). *Left*: A low- $\beta$  case to which Roberts and Taylor’s result is expected to apply. *Right*: A high- $\beta$  case where compressibility and electromagnetic effects are important.

gyroviscosity even when  $\bar{\nu}/\bar{\Omega} = k^2 \rho_i^2/2 \ll 1$ . This is possible because of the relatively slow growth rate of the gravitational instability, even in the ideal limit [1]. Finally, figure 3d shows the cutoff value when the Hall term is included, but the  $v_*$  approximation for gyroviscosity is used. (This approximation is discussed in section III C.) A comparison of figures 3a and 3d shows that the  $v_*$  approximation is evidently quite accurate for this instability, in the limit that we are considering.

It is important to realize that it is not the case that, in these diagrams, neglecting the gyroviscous stress is equivalent to letting  $\bar{\nu} = 0$ , nor is it the case that neglecting the Hall effect is equivalent to letting  $\bar{\Omega}^{-1} = 0$ . In equation (15), terms due entirely to gyroviscosity or the Hall effect are explicitly proportional to  $\bar{\nu}$  or  $\bar{\Omega}^{-1}$ , respectively, only because we suppress other occurrences of these factors by the introduction of the dependent variable  $\bar{g}$  there.

## 2. Linear Simulation results

Our simulation domain has dimensions  $L_x \times L_y$ , with periodic boundaries at  $x = \pm L_x/2$  and conducting, no-slip boundaries at  $y = \pm L_y/2$ . The dimensions are chosen to exclude wavenumbers smaller than  $k_x = 2\pi/L_x$  (smaller wavenumbers are more unstable). Dissipative terms can strongly affect the growth rate, but we are able to simulate the linear regime

stably with  $\eta = \mu = 0$ . The density gradient scale length is taken to be large ( $L_n \gg L_y$ ) to keep the equilibrium fields approximately constant over the entire box.

To measure the growth rate in our simulations, we begin with a small ( $\epsilon \sim 10^{-6}$ ) perturbation in density with  $k_x = 2\pi/L_x$  and  $k_y = \pi/L_y$ . The simulation is allowed to proceed until the growth rate of the density and stream function perturbations equalize and become independent of time. The growth rate is measured by

$$\gamma = \frac{1}{2} \frac{\partial}{\partial t} \ln \left[ \int_0^{L_x} dx A^2(x, y = 0, t) \right] \quad (16)$$

where  $A$  is the density or the stream function. The data points in the figures actually represent the average of the density and stream function growth rates, and the discrepancy between the two values is illustrated by the error bars (this discrepancy is generally smaller than the data point symbol itself).

We present two distinct cases here: a low- $\beta$  case to which Roberts and Taylor’s result is applicable, and a high- $\beta$  case in which the effects of compressibility and electromagnetism are important. Specifically, for the low- $\beta$  case, we choose  $L_x = 2\pi/10$ ,  $L_y = 1$ ,  $L_n = 100$ ,  $g = 0.005$ , and  $I_0 = 100$ . For the high- $\beta$  case, we choose  $L_x = 2\pi/0.05$ ,  $L_y = \pi/0.01$ ,  $L_n = 10^5$ ,  $g = 0.0005$ , and  $I_0 = 1$ . In both cases,  $n_0 = 1$ . As expected, Roberts and Taylor’s result is fairly accurate only for the low- $\beta$  case (the discrepancy is due to the fact that  $k_y = 0$  in Roberts and Taylor’s analysis). In both cases the simulation results are quite close to the exact solution to equation (15).

### 3. *Nonlinear Simulation Results*

As a test of the nonlinear capabilities of our numerical method, we have run simulations of the gravitational instability far into the nonlinear regime. The parameters for these simulation are  $I_0 = 20$ ,  $L_n = 100$ ,  $g = 0.05$ ,  $p_0 = 0.5$ ,  $\eta = 10^{-3}$ ,  $\mu = 10^{-5}$ ,  $\kappa = 10^{-5}$ , and  $\Delta t = 800 \Omega_i^{-1}$ . The simulations are started with a density perturbation ( $\epsilon = 10^{-3}$ ), and allowed to proceed until the density gradient is essentially quenched.

Images of the density profile at an advanced time are shown in figure 6. In the figure, the inclusion of gyroviscosity can be seen to cause the density perturbation to advect in the  $x$ -direction. This is due to the “gyroviscous cancellation” effect, which is discussed in more detail in section III C. The shear in this advection velocity is due to the fact that the

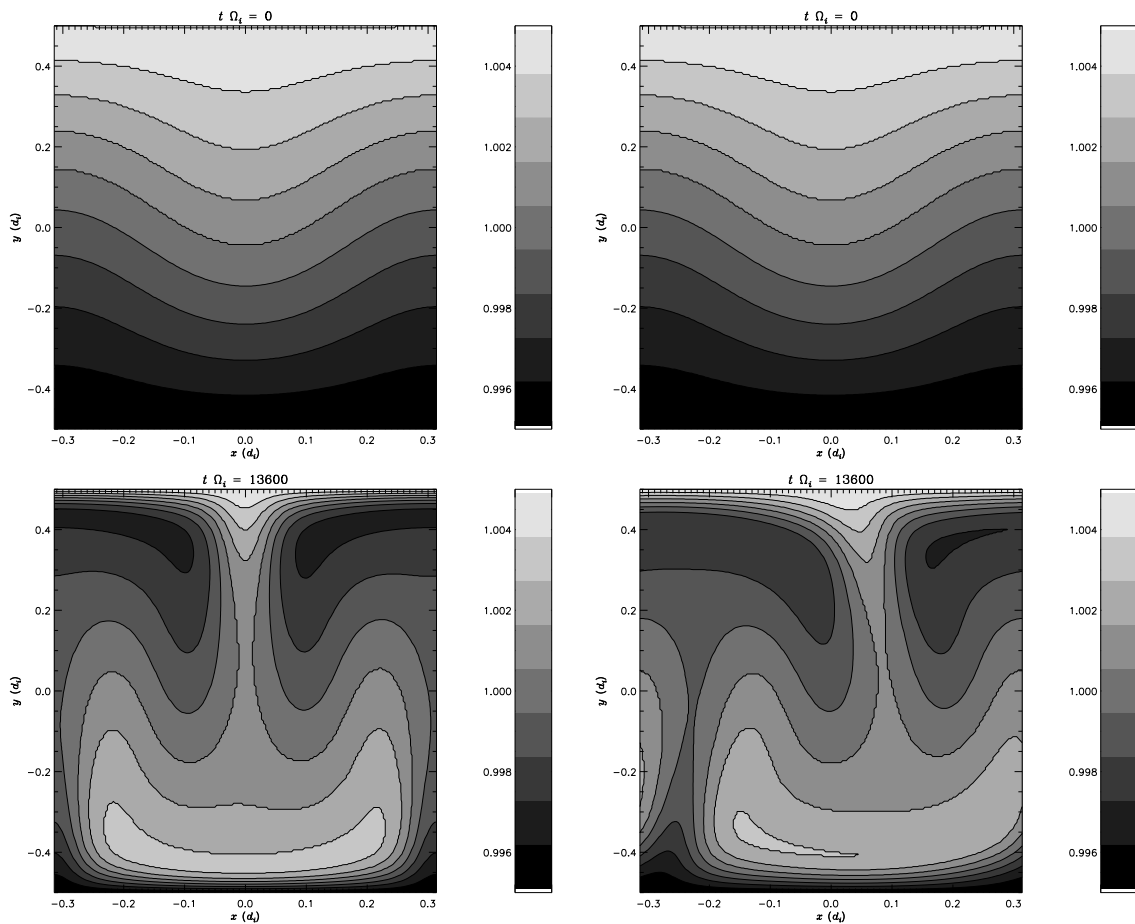


FIG. 5: The density profile from nonlinear simulations of the gravitational instability are shown. The two frames on the left are from a simulation with gyroviscosity turned off; the two on the right include gyroviscosity. The horizontal motion in the simulation including gyroviscosity is due ultimately to the gyroviscous cancellation effect.

magnetization velocity  $v_*$  is not constant over the simulation domain, and to the no-slip boundary conditions. This shear is *not* responsible for the stabilization of the gravitational instability (e.g. by shearing apart nascent convection cells) in this regime, where  $k_y L_n \gg 1$ .

### C. Gyroviscous Cancellation

Frequently the gyroviscous stress is approximated by

$$\nabla \cdot \Pi \approx -n \vec{v}_* \cdot \nabla \vec{v}. \quad (17)$$

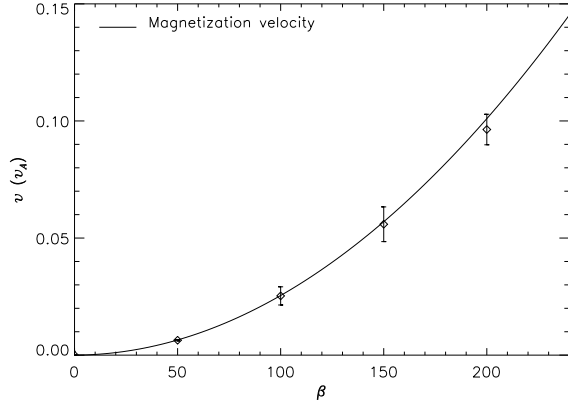


FIG. 6: The phase velocity of a perturbation in  $U$  is plotted against the absolute value of the ion magnetization velocity. If the gyroviscous force is neglected, the perturbation remains stationary.

In this approximation, moving the gyroviscous term to the left-hand side of the fluid momentum equation yields the well known “gyroviscous cancellation” [11]:

$$n(\dot{\vec{v}} + \vec{v} \cdot \nabla \vec{v}) + \nabla \cdot \Pi \approx n[\dot{\vec{v}} + (\vec{v} - \vec{v}_*) \cdot \nabla \vec{v}]. \quad (18)$$

That is, the gyroviscous force acts to “cancel” the velocity at which the fluid velocity is advected, by an amount  $\vec{v}_*$ . It is often assumed that  $\vec{v}_*$  is the diamagnetic drift velocity but, as Ramos points out [11], this is only true when the magnetic field is constant. A more general choice for  $\vec{v}_*$  is the ion magnetization velocity,

$$\vec{v}_* = -\frac{1}{ne} \nabla \times \left( \frac{p^{(i)} \vec{B}}{B^2} \right). \quad (19)$$

To observe the gyroviscous cancellation phenomenon, we consider an equilibrium in which the fluid velocity is zero but the magnetization velocity is nonzero. Specifically, we use the same equilibrium described by equations (13), letting  $g = 0$  (*i.e.* no gravity),  $I_0 = 1$ ,  $L_n = 10^5$ ,  $L_x = 2\pi/0.05$ , and  $L_y = \pi/0.01$ . We then apply a small ( $\epsilon = 10^{-6}$ ) sinusoidal perturbation to  $U$ , and measure the phase velocity of the perturbation. With the gyroviscous force not included, the crest of the perturbation is observed to remain stationary. That is, the perturbation is advected by the fluid velocity  $\vec{v} \approx 0$ . When the gyroviscous force is included, the phase velocity of the perturbation is indeed observed to be approximately  $\vec{v} - \vec{v}_* \approx -\vec{v}_*$ . In figure 6, the measured phase velocity is plotted against the absolute value of the magnetization velocity. It should be emphasized that for this equilibrium, the

contribution of the diamagnetic velocity to  $\vec{v}_*$  is smaller than the contribution due to the gradient in  $\vec{B}$  by a factor  $\beta/2$ —which, for the parameters plotted in figure 6, is up to two orders of magnitude. Therefore the diamagnetic velocity is an extremely poor approximation to  $\vec{v}_*$  in this case.

Re-deriving the linear dispersion relation of the gravitational instability using equation (17) instead of the Braginskii form of the gyroviscous stress simply gives equation (15) with the  $2\bar{v}\bar{g}\bar{\omega}$  term omitted. For the cases simulated in section III B, this turns out to be fairly accurate, differing from the solid curves plotted in figure 4 by only a few percent.

However, there are other situations in which the  $v_*$  approximation is completely inadequate. Consider a homogeneous equilibrium with constant density  $n_0$ , pressure  $p_0$ , and guide field  $I_0$ . Now perturb the stream function  $U_1$  such that

$$U_1 = \epsilon \cos(k_x x). \quad (20)$$

In this scenario,  $\vec{v}_* = 0$ , since there is no gradient in the ion pressure or magnetic field. However, evaluating the full form of Braginskii’s gyroviscous stress, one finds

$$\nabla \cdot \Pi = \frac{p^{(i)} \nabla (\nabla^2 U)}{2I_0}. \quad (21)$$

This is a purely compressional force, and is a linear function of velocity. In the absence of this term, there is no compressional force at all. The results of simulations of this scenario are illustrated in figure 7. The parameters for those simulations are:  $p_0 = p_0^{(i)} = 0.1$ ,  $I_0 = 2$ ,  $k_x = 2\pi$ ,  $\epsilon = 10^{-4}$ , and  $\mu = \eta = 0$ . In the figure, the data points labeled “no gyroviscosity” would be the result of a simulation employing the  $v_*$  approximation to the stress tensor.

#### IV. SUMMARY AND CONCLUSIONS

We have used the method described in section II to include the full form of Braginskii’s gyroviscous stress into our numerical extended-MHD model. To validate this implementation, we have derived the linear dispersion relation of the full eight-field extended-MHD model, including the full gyroviscous stress, for plane waves in a homogeneous plasma, and shown that our numerical simulations converge to values obtained from the dispersion relations.

We have also revisited the gravitational instability, the stabilization of which provides clear evidence of the effect of the gyroviscous stress. We have substantially generalized the

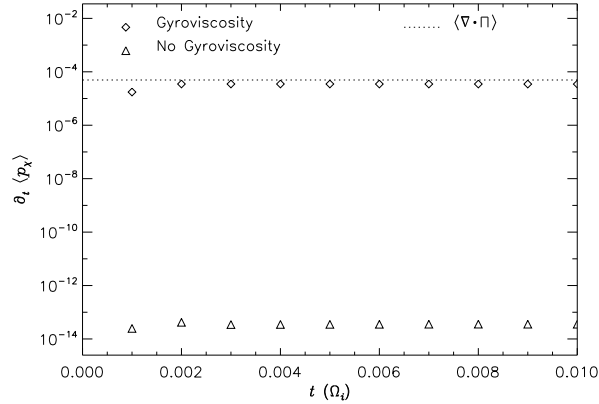


FIG. 7: The domain-averaged compressional force is plotted as a function of time. Without gyroviscosity, this force is due to truncation error only. The  $v_*$  approximation would produce the same results as “no gyroviscosity.”

treatment of Roberts and Taylor [2] to include high- $\beta$  regimes and the effects of electromagnetism. In the linear regime, our numerical simulations are shown to agree closely with our linear theory of this instability. It is worth repeating that for some parameter regimes, this mode is stabilized by gyroviscosity even when  $k\rho_i \ll 1$ .

Finally, we have demonstrated the “gyroviscous cancellation,” with our numerical simulations, and explored some of the implications of using the  $v_*$  approximation instead of the full Braginskii form of gyroviscosity. Evidently this approximation is adequate for understanding the effect of gyroviscosity on the gravitational instability, at least in the limits we have considered, when  $\vec{v}_*$  is taken to be the ion magnetization velocity. We have clearly shown that it can be a poor approximation to use the diamagnetic velocity for  $\vec{v}_*$  in the presence of a magnetic field gradient.

The effect of gyroviscosity on other phenomena in which it might be expected to play an important role, such as low guide field reconnection [10], will be the subject of future work.

## Acknowledgments

The authors thank J. Ramos for useful conversations about the gyroviscous stress; D. Schnack for his suggestion to use the gravitational instability to benchmark implementations of the gyroviscous stress, and for his analysis of Roberts and Taylor’s result; and

J. Breslau for his support regarding numerical methods. This work was supported by U.S. Department of Energy contract DE-AC02-76CH03073.

## APPENDIX A: EXPLICIT CALCULATION OF MATRICES FOR FINITE ELEMENTS WITH POLYNOMIAL BASIS FUNCTIONS

We now specialize to the case in which the basis functions are polynomials of the local coordinates,  $\xi_e$  and  $\eta_e$ , for the finite element indexed by  $e$ :

$$\nu_i = g_{epi} \xi_e^{m_p} \eta_e^{n_p} \quad (\text{A1})$$

where  $g_{epi}$  is constant in space. Furthermore, the local coordinates are taken to be related to the global coordinates through a simple rotation parametrized by  $\theta_e$ :

$$\xi_e = x \cos \theta_e + y \sin \theta_e \quad (\text{A2a})$$

$$\eta_e = -x \sin \theta_e + y \cos \theta_e. \quad (\text{A2b})$$

We then define

$$F_e(m, n) = \int dA_e \xi_e^m \eta_e^n \quad (\text{A3})$$

where  $dA_e = d\xi_e d\eta_e$  is the domain of finite element  $e$ . Using this definition, the  $\vec{L}$  and  $\vec{R}$  matrices can be written algebraically. For example,

$$\begin{aligned} \int dA \nu_i n \nabla^2 U &= \int dA \nu_i \nabla^2 (\nu_j U_j) \nu_k n_k \\ &= \sum_{e=1}^E \int dA_e \nu_i \nabla^2 (\nu_j U_j) \nu_k n_k \\ &= \sum_{e=1}^E g_{epi} g_{eqj} g_{esk} U_j n_k \times \\ &\quad \times [m_q(m_q - 1) F_e(m_t - 2, n_t) + \\ &\quad + n_q(n_q - 1) F_e(m_t, n_t - 2)]. \end{aligned}$$

where  $m_t = m_p + m_q + m_r$  and  $n_t = n_p + n_q + n_r$ . The matrices used in our code, with the exception of the ones arising from the implementation of the gyroviscous force—the  $G$  matrices—have been computed before [5, 6]. The computation of the  $G$  matrices is slightly more involved, because some of them are not coordinate-invariant. Suppressing the subscript  $e$ , we find:

$$\begin{aligned}
G_{ijkl}^{(11a)} &= g \left\{ \begin{array}{l} F_{3,1} [m_p m_q (n_p (m_q - 1) - n_q (m_p - 1))] - \\ - F_{1,3} [n_p n_q (m_p (n_q - 1) - m_q (n_p - 1))] \end{array} \right\} \\
G_{ijkl}^{(12a)} &= \frac{1}{2} g \left\{ \begin{array}{l} F_{3,1} [\frac{1}{2} m_p (m_p - 1) (m_r n_q + m_q n_r) - m_p n_p m_q m_r] - \\ - F_{1,3} [\frac{1}{2} n_p (n_p - 1) (n_r m_q + n_q m_r) - n_p m_p n_q n_r] \end{array} \right\} \\
G_{ijkl}^{(12b)} &= g (m_r n_q - m_q n_r) \left\{ \frac{1}{2} \cos(2\theta) [m_p (m_p - 1) F_{3,1} - n_p (n_p - 1) F_{1,3}] - \sin(2\theta) m_p n_p F_{2,2} \right\} \\
G_{ijkl}^{(12c)} &= g (m_r n_q - m_q n_r) \left\{ \frac{1}{2} \sin(2\theta) [m_p (m_p - 1) F_{3,1} - n_p (n_p - 1) F_{1,3}] + \cos(2\theta) m_p n_p F_{2,2} \right\} \\
G_{ijkl}^{(13a)} &= -\frac{1}{2} g \left\{ \begin{array}{l} F_{4,0} [m_p (m_p - 1) m_q (m_q - 1)] + \\ + F_{0,4} [n_p (n_p - 1) n_q (n_q - 1)] + \\ + F_{2,2} [4 m_p m_q n_p n_q - (m_p (m_p - 1) n_q (n_q - 1) + n_p (n_p - 1) m_q (m_q - 1))] \end{array} \right\} \\
G_{ijkl}^{(13b)} &= g \left\{ \begin{array}{l} \frac{1}{2} \cos(2\theta) \left[ \begin{array}{l} m_p (m_p - 1) (m_q (m_q - 1) F_{4,0} + n_q (n_q - 1) F_{2,2}) - \\ - n_p (n_p - 1) (m_q (m_q - 1) F_{2,2} + n_q (n_q - 1) F_{0,4}) \end{array} \right] - \\ - \sin(2\theta) m_p n_p [m_q (m_q - 1) F_{3,1} + n_q (n_q - 1) F_{1,3}] \end{array} \right\} \\
G_{ijkl}^{(13c)} &= g \left\{ \begin{array}{l} \frac{1}{2} \sin(2\theta) \left[ \begin{array}{l} m_p (m_p - 1) (m_q (m_q - 1) F_{4,0} + n_q (n_q - 1) F_{2,2}) - \\ - n_p (n_p - 1) (m_q (m_q - 1) F_{2,2} + n_q (n_q - 1) F_{0,4}) \end{array} \right] + \\ + \cos(2\theta) m_p n_p [m_q (m_q - 1) F_{3,1} + n_q (n_q - 1) F_{1,3}] \end{array} \right\} \\
G_{ijkl}^{(22a)} &= \frac{1}{4} g (m_p n_q - m_q n_p) F_{1,1} \\
G_{ijkl}^{(23a)} &= -\frac{1}{2} g \left\{ \begin{array}{l} F_{4,0} [m_p m_q (m_q - 1) m_r] + \\ + F_{0,4} [n_p n_q (n_q - 1) n_r] + \\ + F_{2,2} [m_q n_q (m_p n_r + m_r n_p)] \end{array} \right\} \\
G_{ijkl}^{(23b)} &= \frac{1}{2} g [m_q n_q (m_r n_p + m_p n_r) - (m_p m_r n_q (n_q - 1) + n_p n_r m_q (m_q - 1))] F_{2,2} \\
G_{ijkl}^{(33b)} &= g \left\{ \begin{array}{l} \cos(2\theta) \left[ \begin{array}{l} F_{3,1} m_p m_q [(m_p - 1) n_q - n_p (m_q - 1)] + \\ + F_{1,3} n_p n_q [(n_p - 1) m_q - m_p (n_q - 1)] \end{array} \right] - \\ - \sin(2\theta) [m_p (m_p - 1) n_q (n_q - 1) - n_p (n_p - 1) m_q (m_q - 1)] F_{2,2} \end{array} \right\} \\
G_{ijkl}^{(33c)} &= g \left\{ \begin{array}{l} \sin(2\theta) \left[ \begin{array}{l} F_{3,1} m_p m_q [(m_p - 1) n_q - n_p (m_q - 1)] + \\ + F_{1,3} n_p n_q [(n_p - 1) m_q - m_p (n_q - 1)] \end{array} \right] + \\ + \cos(2\theta) [m_p (m_p - 1) n_q (n_q - 1) - n_p (n_p - 1) m_q (m_q - 1)] F_{2,2} \end{array} \right\}
\end{aligned}$$

where  $g = g_{pi}g_{qj}g_{rk}g_{sl}$  and  $F_{a,b} = F(m_p + m_q + m_r + m_s - a, n_p + n_q + n_r + n_s - b)$ .

---

- [1] M. N. Rosenbluth, N. A. Krall, and N. Rostoker, Nucl. Fusion Suppl. **1**, 143 (1962).
- [2] K. V. Roberts and J. B. Taylor, Phys. Rev. Lett. **8**, 197 (1962).
- [3] W. Park, E. V. Belova, G. Y. Fu, X. Z. Tang, H. R. Strauss, and L. E. Sugiyama, Phys. Plasmas **6**, 1796 (1999).
- [4] A. H. Glasser, C. R. Sovinec, R. A. Nebel, T. A. Gianakon, S. J. Plimpton, M. S. Chu, D. D. Schnack, and the NIMROD Team, Plasma Phys. Control. Fusion **41**, A747 (1999).
- [5] S. C. Jardin, J. Comp. Phys. **200**, 133 (2004).
- [6] S. C. Jardin and J. A. Breslau, Phys. Plasmas **12**, 056101 (2005).
- [7] R. Fitzpatrick, Phys. Plasmas pp. 937–946 (2004).
- [8] H. P. Furth, J. Killeen, and M. N. Rosenbluth, Phys. Fluids **6**, 459 (1963).
- [9] B. N. Rogers, R. E. Denton, J. F. Drake, and M. A. Shay, Phys. Rev. Lett. **87**, 195004 (2001).
- [10] A. Ishizawa and R. Horiuchi, Phys. Rev. Lett. **95**, 045003 (2005).
- [11] J. J. Ramos, Phys. Plasmas **12**, 112301 (2005).
- [12] S. I. Braginskii, in *Reviews of Plasma Physics*, edited by M. A. Leontovich (Consultants Bureau, New York, 1965), vol. 1, pp. 205–311.
- [13] D. D. Schnack (2005), unpublished note, URL <http://w3.pppl.gov/cemm>.
- [14] A. N. Kaufman, Phys. Fluids **3**, 610 (1960).

## External Distribution

Plasma Research Laboratory, Australian National University, Australia  
Professor I.R. Jones, Flinders University, Australia  
Professor João Canalle, Instituto de Fisica DEQ/IF - UERJ, Brazil  
Mr. Gerson O. Ludwig, Instituto Nacional de Pesquisas, Brazil  
Dr. P.H. Sakanaka, Instituto Fisica, Brazil  
The Librarian, Culham Science Center, England  
Mrs. S.A. Hutchinson, JET Library, England  
Professor M.N. Bussac, Ecole Polytechnique, France  
Librarian, Max-Planck-Institut für Plasmaphysik, Germany  
Jolan Moldvai, Reports Library, Hungarian Academy of Sciences, Central Research  
Institute for Physics, Hungary  
Dr. P. Kaw, Institute for Plasma Research, India  
Ms. P.J. Pathak, Librarian, Institute for Plasma Research, India  
Dr. Pandji Triadyaksa, Fakultas MIPA Universitas Diponegoro, Indonesia  
Professor Sami Cuperman, Plasma Physics Group, Tel Aviv University, Israel  
Ms. Clelia De Palo, Associazione EURATOM-ENEA, Italy  
Dr. G. Grosso, Istituto di Fisica del Plasma, Italy  
Librarian, Naka Fusion Research Establishment, JAERI, Japan  
Library, Laboratory for Complex Energy Processes, Institute for Advanced Study,  
Kyoto University, Japan  
Research Information Center, National Institute for Fusion Science, Japan  
Professor Toshitaka Idehara, Director, Research Center for Development of Far-Infrared Region,  
Fukui University, Japan  
Dr. O. Mitarai, Kyushu Tokai University, Japan  
Mr. Adefila Olumide, Ilorin, Kwara State, Nigeria  
Dr. Jiangang Li, Institute of Plasma Physics, Chinese Academy of Sciences, People's Republic of China  
Professor Yuping Huo, School of Physical Science and Technology, People's Republic of China  
Library, Academia Sinica, Institute of Plasma Physics, People's Republic of China  
Librarian, Institute of Physics, Chinese Academy of Sciences, People's Republic of China  
Dr. S. Mirnov, TRINITI, Troitsk, Russian Federation, Russia  
Dr. V.S. Strelkov, Kurchatov Institute, Russian Federation, Russia  
Kazi Firoz, UPJS, Kosice, Slovakia  
Professor Peter Lukac, Katedra Fyziky Plazmy MFF UK, Mlynska dolina F-2, Komenskeho Univerzita,  
SK-842 15 Bratislava, Slovakia  
Dr. G.S. Lee, Korea Basic Science Institute, South Korea  
Dr. Rasulkhozha S. Sharafiddinov, Theoretical Physics Division, Institute of Nuclear Physics, Uzbekistan  
Institute for Plasma Research, University of Maryland, USA  
Librarian, Fusion Energy Division, Oak Ridge National Laboratory, USA  
Librarian, Institute of Fusion Studies, University of Texas, USA  
Librarian, Magnetic Fusion Program, Lawrence Livermore National Laboratory, USA  
Library, General Atomics, USA  
Plasma Physics Group, Fusion Energy Research Program, University of California at San Diego, USA  
Plasma Physics Library, Columbia University, USA  
Alkesh Punjabi, Center for Fusion Research and Training, Hampton University, USA  
Dr. W.M. Stacey, Fusion Research Center, Georgia Institute of Technology, USA  
Director, Research Division, OFES, Washington, D.C. 20585-1290

The Princeton Plasma Physics Laboratory is operated  
by Princeton University under contract  
with the U.S. Department of Energy.

Information Services  
Princeton Plasma Physics Laboratory  
P.O. Box 451  
Princeton, NJ 08543

Phone: 609-243-2750  
Fax: 609-243-2751  
e-mail: [pppl\\_info@pppl.gov](mailto:pppl_info@pppl.gov)  
Internet Address: <http://www.pppl.gov>